AMERICAN SOCIETY FOR MICROBIOLOGY | Infection and Immunity

# Distinct Prominent Roles for Enzymes of *Plasmodium berghei* Heme Biosynthesis in Sporozoite and Liver Stage Maturation

**Zaira Rizopoulos,[a] Kai Matuschewski,[a,b] Joana M. Haussig[a]**

Parasitology Unit, Max Planck Institute for Infection Biology, Berlin, Germany[a]; Department of Molecular Parasitology, Institute of Biology, Humboldt University, Berlin, Germany[b]

**Malarial parasites have evolved complex regulation of heme supply and disposal to adjust to heme-rich and -deprived host environments. In addition to its own pathway for heme biosynthesis, *Plasmodium* likely harbors mechanisms for heme scavenging from host erythrocytes. Elaborate compartmentalization of *de novo* heme synthesis into three subcellular locations, including the vestigial plastid organelle, indicates critical roles in life cycle progression. In this study, we systematically profile the essentiality of heme biosynthesis by targeted gene deletion of enzymes in early steps of this pathway. We show that disruption of endogenous heme biosynthesis leads to a first detectable defect in oocyst maturation and sporogony in the *Anopheles* vector, whereas blood stage propagation, colonization of mosquito midguts, or initiation of oocyst development occurs indistinguishably from that of wild-type parasites. Although sporozoites are produced by parasites lacking an intact pathway for heme biosynthesis, they are absent from mosquito salivary glands, indicative of a vital role for heme biosynthesis only in sporozoite maturation. Rescue of the first defect in sporogony permitted analysis of potential roles in liver stages. We show that liver stage parasites benefit from but do not strictly depend upon their own aminolevulinic acid synthase and that they can scavenge aminolevulinic acid from the host environment. Together, our experimental genetics analysis of *Plasmodium* enzymes for heme biosynthesis exemplifies remarkable shifts between the use of endogenous and host resources during life cycle progression.**

Heme is a ubiquitous iron-porphyrin complex that serves as a cofactor of hemoproteins, such as globins, catalases, and cytochromes (1). The iron component of heme permits the binding of diatomic gases, as well as unique enzymatic redox reactions based on its reduction potential from the oxidized ferric ($Fe^{3+}$) to the reduced ferrous ($Fe^{2+}$) state (1). Thus, heme mediates fundamental biological processes, including oxygen transport, antioxidant responses, and cellular respiration, and is, therefore, indispensable for virtually all living organisms. Exceptions, like the parasitic kinetoplastid flagellate *Phytomonas serpens* that can survive in the complete absence of heme (2), are rare. As a result of this nearly universal dependence on heme, two complementary strategies for heme acquisition have evolved; heme scavenging and *de novo* heme biosynthesis.

*Plasmodium* parasites are the causative agents of malaria and have adapted to an intraerythrocytic lifestyle during blood infection, the exclusive pathogenic phase of the parasite life cycle. Erythrocytes make up the largest pool of heme in the human body, as they are rich in hemoglobin. In turn, hemoglobin constitutes the major source of amino acids for developing blood stage parasites, which import and digest almost all host hemoglobin, liberating large amounts of heme (3). Free heme acts as a biological Fenton reagent and can thus damage organic molecules by oxidation (4). Therefore, *Plasmodium* needs to detoxify free heme by biopolymerization to a crystalline pigment termed hemozoin (5). Accordingly, *Plasmodium* parasites have evolved a convoluted regulation of heme metabolism to adjust to heme-rich and heme-deprived host environments during their complex life cycle (6).

*Plasmodium* has the capacity to produce its own heme and possesses all necessary enzymes for *de novo* heme biosynthesis (7). *Plasmodium* heme biosynthesis is unique to its phylum, since it extends to three cellular compartments, i.e., the cytoplasm, the mitochondrion, and the apicoplast (8). The apicoplast is a relict, nonphotosynthetic plastid found in most apicomplexan parasites and originates from a secondary endosymbiotic event (9). Three *Plasmodium falciparum* enzymes of the heme biosynthesis pathway localize to this organelle: (i) δ-aminolevulinic acid dehydratase (ALAD) (10), (ii) porphobilinogen deaminase (PBGD) (11), and (iii) uroporphyrinogen III carboxylase (UROD) (12) (Fig. 1A). The potential advantage for compartmentalization of these three enzymes, which are typically cytoplasmic, remains enigmatic. All other enzymes in the pathway, such as the mitochondrial aminolevulinic acid synthase (ALAS), which catalyzes the first and rate-limiting step, display a standard subcellular distribution between mitochondrion and cytoplasm (13–15) (Fig. 1A).

Several putative *Plasmodium* hemoproteins have been identified bioinformatically (7) or by studies of *in vitro* binding to recombinant proteins (6). However, the biological significance of most of these proteins and their interaction with heme remains largely unknown. To date, heme is considered to be primarily required by cytochromes of the electron transport chain (ETC) for mitochondrial respiration (8, 16). The *Plasmodium* ETC has long been recognized as a vulnerable target for antimalarial drugs (17, 18). Atovaquone-proguanil, which is primarily used for presumptive treatment during short-term visits to countries where malaria

**Received** 25 February 2016 **Returned for modification** 9 April 2016
**Accepted** 29 August 2016

**Accepted manuscript posted online** 6 September 2016

**Citation** Rizopoulos Z, Matuschewski K, Haussig JM. 2016. Distinct prominent roles for enzymes of *Plasmodium berghei* heme biosynthesis in sporozoite and liver stage maturation. Infect Immun 84:3252–3262. doi:10.1128/IAI.00148-16.

**Editor:** J. H. Adams, University of South Florida

Address correspondence to Zaira Rizopoulos, rizopoulos@mpiib-berlin.mpg.de.

Supplemental material for this article may be found at http://dx.doi.org/10.1128/IAI.00148-16.

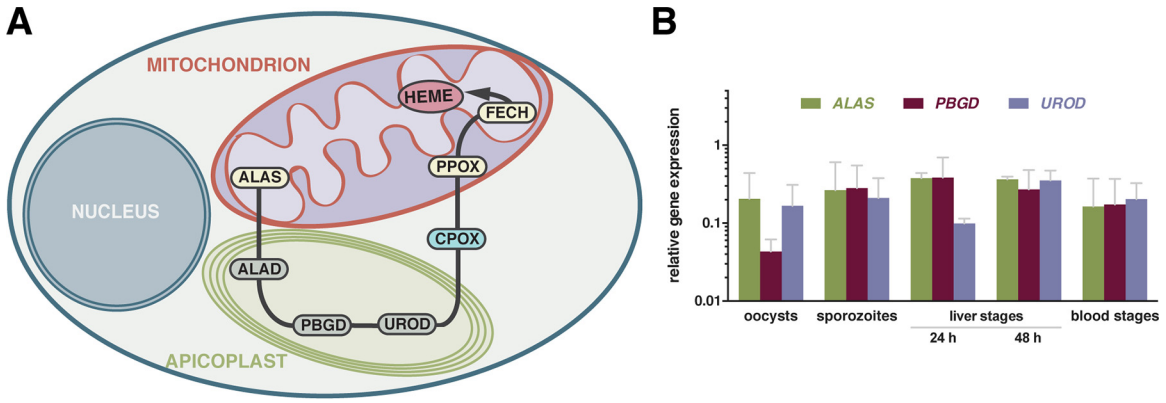


**FIG 1** Ubiquitous expression of three *Plasmodium berghei* genes that encode early steps of heme biosynthesis. (A) Overview of the *Plasmodium* heme biosynthesis pathway. Heme (red) is synthesized from eight molecules of δ-aminolevulinic acid by sequential enzymes distributed in the mitochondrion (yellow), the apicoplast (gray), and the cytoplasm (blue). ALAS, δ-aminolevulinic acid synthase; ALAD, δ-aminolevulinic acid hydratase; PBGD, porphobilinogen deaminase; UROD, uroporphyrinogen III decarboxylase; CPOX, coproporphyrinogen oxidase; PPOX, protoporphyrinogen oxidase; FECH, ferrochelatase. (B) Expression profiling of selected transcripts of the *Plasmodium* heme biosynthesis pathway. RNAs isolated from day 10 oocysts, salivary gland sporozoites, cultured infected hepatoma cells (24 or 48 h after infection), and mixed blood stages were analyzed by RT-qPCR using primers specific for *ALAS*, *PBGD*, and *UROD*. Expression was normalized to the average levels of *HSP70-1* and *GFP* transcripts. Shown is the mean expression (±standard deviation) from two independent experiments, done in triplicate. Differences in expression between genes and between life cycle stages were not significant ($P > 0.1$; two-way analysis of variance).

is endemic, inhibits the cytochrome $bc_1$ complex (19–21). Interestingly, the antimalarial activity of atovaquone-proguanil strictly depends on arrest of the pyrimidine biosynthesis pathway by indirect inhibition of *Plasmodium* dihydroorotate dehydrogenase, which relies on the ETC to recycle electrons (17, 22). On the other hand, the respiratory activity of the *Plasmodium* ETC is essential during parasite development in the *Anopheles* vector, as shown by normal blood stage growth and complete arrest of oocyst development in *Plasmodium berghei* mutants that contain targeted deletions of type II NADH:ubiquinone dehydrogenase or the ATP synthase β subunit (23, 24).

Recent reports (25, 26) have refuted the longstanding notion that *Plasmodium de novo* heme biosynthesis is essential for blood stage development (27). Strikingly, heme scavenging from host erythrocytes is important for parasite growth, as shown by refractoriness to *P. falciparum* growth within ferrochelatase (FECH)-deficient erythrocytes from individuals with erythropoietic protoporphyria (28). In good agreement with these natural genetics data, vestigial heme synthesis in host erythrocytes can be exploited for host-directed therapy of malaria (29).

As expected from the vital role of the *Plasmodium* ETC in the mosquito vector, *P. berghei* and *P. falciparum* parasites that contain targeted deletions of *ALAS* and of *FECH*, which catalyzes the ultimate step in heme synthesis, displayed a complete arrest in vector stage development (25, 26). Phenocopy of impaired cellular respiration by a dysfunctional heme biosynthesis is consistent with the notion that *Plasmodium* hemoproteins function exclusively in the ETC.

Loss of *ALAS* function could be rescued by exogenous supply of aminolevulinic acid (ALA) and permitted the phenotypic analysis of heme biosynthesis beyond sporogony (25). The authors reported a second, strictly essential role for heme synthesis in liver stage development, but no conclusive evidence by robust assays was provided. Therefore, the extent and details of a role for *Plasmodium* heme biosynthesis in the liver stage remain elusive. Furthermore, a potential contribution of the hepatocyte host pathway has not been excluded. Together, the present data suggest a complex interplay between endogenous biosynthesis and auxotrophy of heme during different phases of the life cycle. Because of the therapeutic potential of targeting the acquisition of this indispensable molecule, further insights into the essentiality of *Plasmodium* heme biosynthesis and potential scavenging mechanisms are necessary.

In the present study, we profile the essentiality of two apicoplast-localized enzymes of heme biosynthesis, PBGD and UROD, during *P. berghei* life cycle progression and thereby reveal a previously undescribed role in sporozoite production and maturation. Furthermore, we elucidate the role of an enzyme of heme biosynthesis in liver stage development. A detailed analysis of *alas*$^-$ sporozoites explores endogenous heme biosynthesis as a target for causal-prophylactic treatment of *Plasmodium* infections.

## MATERIALS AND METHODS

**Ethics statement.** All animal work was conducted in strict accordance with the German Tierschutzgesetz in der Fassung vom 22. Juli 2009, which implements Directive 2010/63/EU from the European Parliament and Council (On the Protection of Animals Used for Scientific Purposes). The protocol was approved by the ethics committee of the Berlin state authorities (LAGeSo, permit G0469/09).

**Experimental animals, parasites, and cell lines.** Female NMRI and C57BL/6 mice were obtained from Charles River Laboratories (Sulzfeld, Germany). Female Swiss mice were obtained from Janvier Labs (Le Genest-Saint-Isle, France). Sporozoite and merosome infections were performed with C57BL/6 or Swiss mice. All other parasite infections were performed with NMRI mice. For complementation of *alas*$^-$ parasites in mice, the drinking water was supplemented with 0.1% 5-aminolevulinic acid hydrochloride (ALA) (Sigma) at the time of infection. *Anopheles stephensi* mosquitoes were raised under a 14-h-light/10-h-dark cycle at 28°C and 80% humidity and were fed daily on 10% sucrose. Complementation of *alas*$^-$ parasites in mosquitoes was conducted with a 10% sucrose-0.1% ALA feeding solution for durations indicated. Experimental genetics assays were all performed in the *P. berghei* strain ANKA. For the competitive growth assay, the Berred parasite reference line (30) was used as a control. For all other experiments, the GFPcon line (31) was used as a control. For the *in vitro* analysis of *Plasmodium* liver stage development,

human Huh7 hepatoma cells cultured in supplemented Dulbecco's modified Eagle medium (DMEM) were used.

**Generation of recombinant parasite lines.** For the generation of vectors targeting enzymes of the *P. berghei* heme biosynthesis pathway, PBGD (CAAI01000436.1), UROD (CAAI01001735.1), ALAD (CAAI01006632.1), and ALAS (CAAI01001041.1) (pHEME-ko), fragments of the 3′ and 5′ untranslated regions (UTRs) were amplified from genomic DNA (gDNA) using gene-specific primers (see Table S1 in the supplemental material). First, 3′ fragments were cloned into the pBAT vector (32), following restriction digestion with HindIII and KpnI to generate intermediate constructs (pHEME-im). Then, the 5′ UTR fragments were digested with SacII and EcoRV and cloned into the respective SacII- and PvuII-linearized pHEME-im constructs, thus removing the mCherry-3×Myc tag. Finally, the pHEME-ko vectors were linearized with ScaI and SalI before transfection into *P. berghei* strain ANKA (wild-type [wt]) parasites. Isolation of fluorescent parasites was performed as previously described (33). Details on vector construction and genotyping strategies, including primer sequences and restriction endonuclease recognition sites used for molecular cloning, are provided in Fig. 2 and in Table S1 in the supplemental material.

**Genotyping by diagnostic PCR and Southern blotting.** Successful integration was confirmed by standard diagnostic PCR (for primers, see Table S1 in the supplemental material). In addition, genotypes of all isogenic knockout (ko) parasite lines were confirmed by Southern blotting using the PCR DIG probe synthesis kit and the DIG luminescent detection kit (Roche), according to the manufacturer's protocol. For amplification of the hybridization probe, the 3′ homologous sequences used for targeted integration of the transfection vectors (see Table S1) were used. The *pbgd*$^{-}$, *urod*$^{-}$, or *alas*$^{-}$ parasite-specific hybridization probes were annealed to EcoRI-digested gDNA, resulting in bands of 10.3 kb (wt) and 15.3 kb (*pbgd*$^{-}$), 9.8 kb (wt) and 14.8 kb (*urod*$^{-}$), or 6.42 kb (wt) and 13.7 kb (*alas*$^{-}$), respectively.

***Plasmodium* life cycle analysis.** Blood feeding and mosquito dissections were performed as previously described (34). For comparative quantification of green fluorescent protein (GFP)-expressing versus mercurochrome-stained oocysts, mosquito midguts infected with wt parasites were isolated 10 days postinfection. First, midguts were imaged and images were later analyzed based on GFP-positive fluorescent signals. The same midguts were subsequently stained with a 0.5% mercurochrome solution for 10 min, and oocysts were counted. Hemolymph was obtained by gentle lavage with RPMI medium via the thorax of anesthetized mosquitoes after removal of the distal abdominal segment. Midgut-, hemocoel-, and salivary gland-associated sporozoites were quantified at days 14, 16, and 18 to 20 after the infective blood meal, respectively. Bite-back experiments were performed by exposing naive recipient mice to 3 to 9 infected mosquitoes. All other sporozoite infections of mice were performed by intravenous injection into the tail vein of 10,000 sporozoites in RPMI medium supplemented with 3% bovine serum albumin (BSA). Patency and parasitemia were determined by daily examination of Giemsa-stained thin blood smears or by flow cytometry, as previously described (30). The development of signature symptoms of experimental cerebral malaria (ECM) was monitored. Mice were diagnosed with onset of ECM if they showed behavioral and functional abnormalities, such as ataxia, paralysis, or convulsions (35). Mice were sacrificed immediately after a diagnosis of ECM.

**Real-time quantitative PCR (RT-qPCR).** For detection of parasite liver loads, livers of infected mice were removed 42 h after intravenous sporozoite injection. For expression profiling, cDNA preparations from midguts infected with day 10 oocysts, isolated salivary gland sporozoites, infected Huh7 cells, and infected erythrocytes were used. Total RNA was extracted from samples using TRIzol reagent (Invitrogen) or the RNeasy kit (Qiagen) according to the manufacturer's instructions. Reverse transcription was performed using the RETROscript kit (Ambion). Real-time PCR was performed in technical triplicates with the ABI 7500 sequence detection system and Power SYBR green PCR master mix (Applied Biosystems), as described previously (36, 37). Transcript-specific primers for *P. berghei* 18S rRNA and mouse glyceraldehyde-3-phosphate dehydrogenase (GAPDH) were used for analysis of parasite liver load (see Table S1 in the supplemental material). Transcript-specific primers for *P. berghei PBGD*, *UROD*, *ALAS*, *HSP70*, and *GFP* were used for expression analysis (see Table S1). Relative transcript abundance was determined using the threshold cycle ($2^{-\Delta CT}$) method. Expression data were normalized to the ubiquitous endogenous transcript *HSP70-1* (38) and the transgene transcript *GFP* (31), and liver loads were determined relative to the murine *GAPDH* gene (39).

***In vitro* infections and siRNA.** Huh7 cells were seeded on 96-well plates (Greiner) for small interfering RNA (siRNA) transfections and on 8-well chamber slides (Nalge Nunc International) for all other *in vitro* infection experiments and infected with 5,000 or 10,000 sporozoites per well, respectively. For siRNA knockdown, hepatoma cells were reverse transfected with 12 nM target-specific or control siRNA sequences (Ambion; see Table S1 in the supplemental material) according to the manufacturer's instructions. Cells were infected 48 h post-siRNA transfection. The knockdown efficiency was assessed 48 h postinfection by RT-qPCR using transcript-specific primers (see Table S1).

**Immunofluorescence and microscopy.** For the analysis of exoerythrocytic forms, samples were fixed 24, 48, or 72 h after infection in −20°C methanol or 4% paraformaldehyde (PFA) and labeled with monoclonal mouse anti-*P. berghei* heat shock protein 70 (*Pb*HSP70) (40) and polyclonal rabbit anti-*P. berghei* upregulated in infectious sporozoite gene 4 (*Pb*UIS4) primary antibodies (41). For the staining of isolated sporozoites, samples were fixed in 4% PFA and permeabilized with 1% Triton X-100. Samples were then labeled with mouse antisporozoite antiserum (kindly provided by Katja Mueller). Primary staining was followed by Alexa 488- or Alexa 546-conjugated secondary antibodies (Invitrogen) and Hoechst 33342 (Invitrogen). Slides were mounted with Fluoromount-G (Southern Biotech). For the analysis of merosomes, samples were harvested 72 h after infection by centrifugation and counted in a Neubauer chamber.

Immunofluorescence assays, infected mosquito midguts, and isolated merosomes were analyzed using a Zeiss Axio Observer.Z1 microscope (Zeiss) equipped with a 5×/0.25, a 10×/0.45, and a 63×/1.2 oil immersion lens. Pictures were collected with an AxioCam MRm (Zeiss) and the Zeiss AxioVision software (Zeiss). Particle analysis and image processing were done with the Fiji ImageJ software package.

## RESULTS

**Expression profiling of *Plasmodium berghei* heme biosynthesis genes.** We first assessed expression of three *Plasmodium* genes that encode enzymes of early steps in heme biosynthesis during life cycle progression (Fig. 1). We quantified transcript levels in representative samples obtained from day 10 oocysts, salivary gland-associated sporozoites, *in vitro*-cultured liver stages, and mixed blood stages (Fig. 1B). With the exception of a slight, albeit nonsignificant, downregulation of *PBGD* in oocysts and of *UROD* in early liver stages, all three genes displayed uniform expression in the invertebrate and vertebrate hosts. This finding indicates that the heme biosynthesis pathway is ubiquitously expressed irrespective of the phase of the *Plasmodium* life cycle.

Heme biosynthesis is an almost universally conserved metabolic pathway. As such, syntenic gene orthologs to *ALAS*, *PBGD*, and *UROD* have been identified in *Plasmodium* species that cause malaria in humans, such as *P. falciparum* and *Plasmodium vivax*, as well as in *Toxoplasma gondii*, the causative agent of toxoplasmosis. A multiple-sequence alignment analysis revealed a high degree of homology between these enzymes in the murine parasite *P. berghei* and all three human pathogens (see Fig. S1 in the supplemental material).

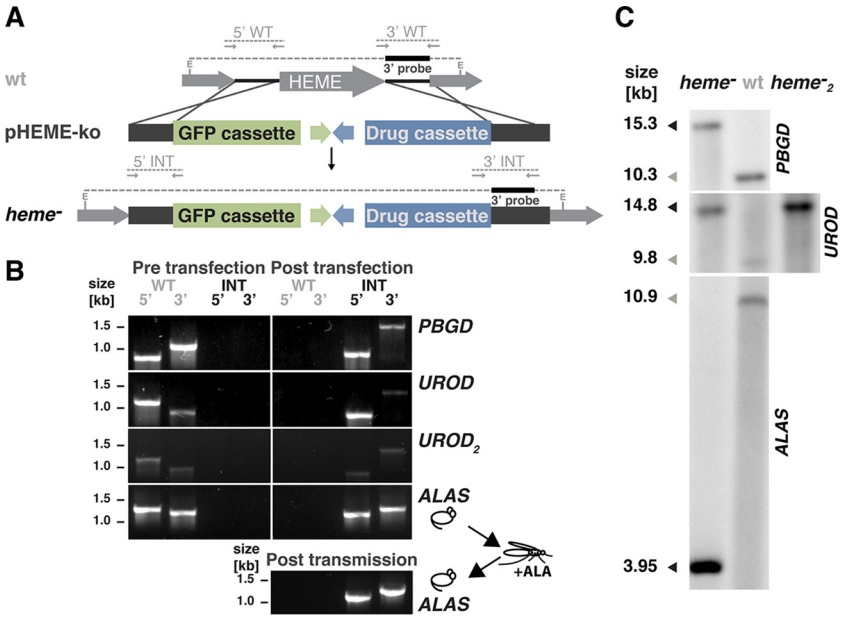


**FIG 2** Targeted deletions of three *P. berghei* genes for heme biosynthesis. (A) Replacement strategy for the deletion of *PBGD*, *UROD*, and *ALAS*. The respective endogenous loci (HEME) were targeted with replacement plasmids (pHEME-ko) containing 5′ and 3′ regions (black) flanking the open reading frame (light gray arrow), a high-expression GFP cassette (green), and the hDHFR-yFcu drug-selectable cassette (blue). Primer combinations specific for integration (5′ and 3′ INT) and wild-type (5′ and 3′ WT) loci, expected PCR fragments, and the Southern blot probe are indicated. (B) Diagnostic PCR-based genotyping of *pbgd*$^{-}$, *urod*$^{-}$, *urod*$^{-}_{2}$, and *alas*$^{-}$ parasites. Results of PCRs of wt before transfection or drug-selected and FACS-sorted parasites after transfection are shown to verify successful deletion. The absence of wt-specific signals in the isogenic lines confirms the purity of the respective knockout parasite populations. Genotyping of *alas*$^{-}$ blood stage parasites shows no presence of wt-specific signals, including after completion of a full round in the life cycle by supplementation of infected *A. stephensi* mosquitoes with aminolevulinic acid (ALA). (C) Southern blot analysis of the isogenic *pbgd*$^{-}$, *urod*$^{-}$, *urod*$^{-}_{2}$, and *alas*$^{-}$ lines. The 3′ homologous sequences used for targeted integration of the transfection vectors (black bar in panel A) were used as probes and hybridized to PstI/NheI or EcoRI restriction-digested gDNA of wt or knockout (*heme*$^{-}$) parasites. The size shifts from wt fragments (gray arrowheads) to integration fragments (black arrowheads) correspond to the predicted fragment lengths (dashed line in panel A).

**Targeted deletion of *P. berghei* apicoplast-localized *PBGD* and *UROD* but refractoriness of *ALAD*.** To assess the functional importance of parasite heme biosynthesis in the apicoplast, we targeted *PBGD* and *UROD* by a genetic replacement strategy in *P. berghei* (Fig. 2A). As inferred from successful deletion of other heme biosynthesis target genes (25, 26) and a successful *PBGD* knockout in *P. falciparum* (29), both genes were readily deleted by double homologous recombination, confirming their dispensable nature during *Plasmodium berghei* blood infection *in vivo*. Next, isogenic *pbgd*$^{-}$ and *urod*$^{-}$ parasite lines were generated through fluorescence-activated cell sorting (FACS) (33). The absence of wild-type (wt) parasites in the isogenic knockout (ko) lines was verified by diagnostic PCR and Southern blot analysis (Fig. 2B and C). To compare the phenotypic profiles of our mutant lines, we generated an additional *alas*$^{-}$ parasite line, as reported previously (25), and an independent *urod*$^{-}$ line, termed *urod*$^{-}_{2}$ (Fig. 2). Additionally, we attempted to delete the third apicoplast-localized heme biosynthesis enzyme, ALAD, but were unsuccessful (see Fig. S2 in the supplemental material), indicating that this gene is indispensable for asexual blood stage growth.

To analyze blood stage fitness of *pbgd*$^{-}$, *urod*$^{-}$, *urod*$^{-}_{2}$, and *alas*$^{-}$ parasites, we performed an intravital competitive growth assay with a red fluorescent parasite reference line (30) (see Fig. S3 in the supplemental material). We observed no significant differences in the blood stage growth rate of ko parasites in comparison to wild type (wt). In conclusion, initial steps of *Plasmodium* heme synthesis in the apicoplast do not play an important role for parasite blood stage propagation *in vivo*.

**Normal mosquito colonization by *pbgd*$^{-}$, *urod*$^{-}$, and *alas*$^{-}$ parasites.** We next followed the life cycle progression of all four mutant parasite lines, *pbgd*$^{-}$, *urod*$^{-}$, *urod*$^{-}_{2}$, and *alas*$^{-}$, in *Anopheles stephensi* mosquitoes. After blood feeding on infected mice, mosquito midguts were dissected and oocyst numbers were quantified based on intrinsic GFP expression (Fig. 3). We noticed high oocyst burdens in all infected mosquitoes, irrespective of the parasite line (Fig. 3A). Comparative quantification of oocyst numbers revealed similar mean numbers for mosquitoes infected with wt, *pbgd*$^{-}$, *urod*$^{-}$, *urod*$^{-}_{2}$, or *alas*$^{-}$ parasites (Fig. 3B). These findings show that disruption of *Plasmodium* heme biosynthesis in the apicoplast does not affect oocyst formation in the mosquito midgut.

Our observations contrast with previous data (25, 26). In these studies, classical mercurochrome staining detected only very few oocysts in mosquitoes infected with *P. berghei alas*$^{-}$ or *fech*$^{-}$ parasites and none in mosquitoes infected with *P. falciparum fech*$^{-}$ parasites. Therefore, we compared the traditional staining protocol to fluorescence-based imaging of transgenic parasites (see Fig. S4 in the supplemental material). Detected oocyst numbers based on GFP fluorescence were always considerably higher than those detected by mercurochrome staining, strengthening the notion that expression of the fluorescent reporter protein GFP permits reliable analysis of mosquito colonization. Together, we can exclude a role for endogenous *Plasmodium* heme biosynthesis in midgut colonization and onset of sporogony.

**Defective oocyst maturation of *pbgd*$^{-}$, *urod*$^{-}$, and *alas*$^{-}$ parasites.** Careful examination of oocysts formed by the four ko lines revealed a consistent and significant size reduction in comparison

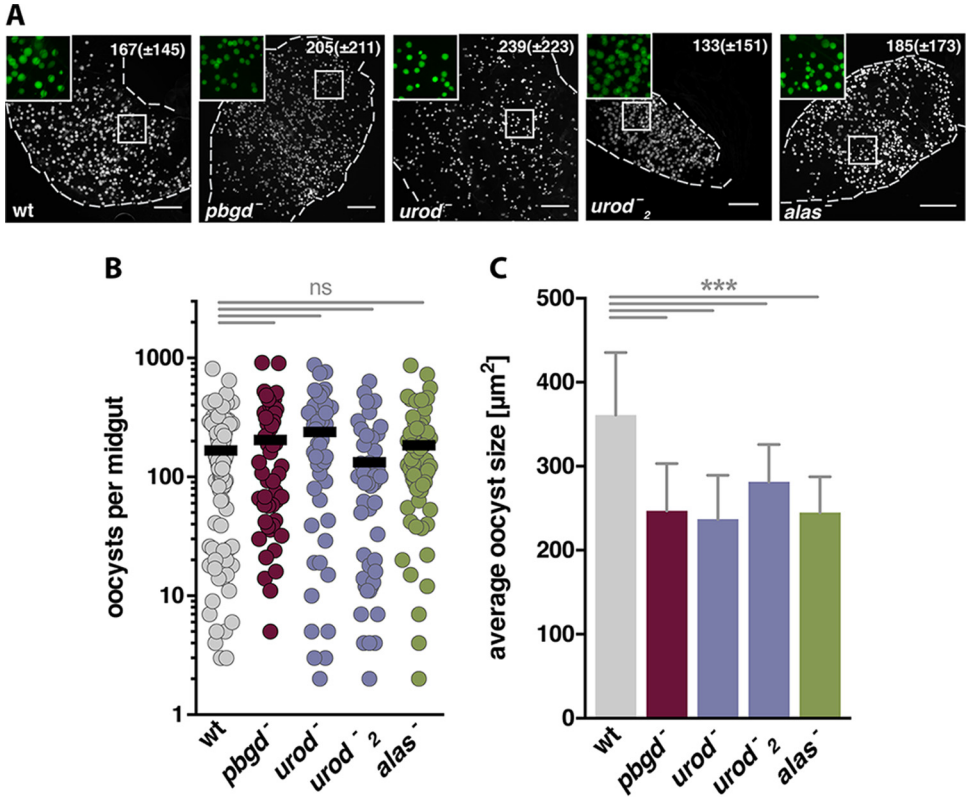


**FIG 3** *Plasmodium* heme biosynthesis is dispensable for mosquito colonization but important for oocyst maturation. (A) Representative images of mosquito midguts infected with wt, *pbgd*$^-$, *urod*$^-$, *urod*$^-_2$, or *alas*$^-$ oocysts. Infected mosquitoes were dissected 10 days after an infective blood meal. Images depict GFP-expressing oocysts. Dashed lines outline the mosquito midguts. Mean oocyst numbers (±standard deviations) from at least four independent mosquito feedings are displayed in the upper right. Bars, 200 μm. (B) Quantification of average oocyst number per infected mosquito for wt and mutant parasite lines. Shown are mean oocyst numbers from at least four independent experiments. Differences were not significant (ns, $P > 0.1$; Kruskal-Wallis test followed by Dunn's posttest). (C) Quantification of mean oocyst size for wt and mutant parasite lines. Shown are mean oocyst sizes (±standard deviations) from at least three independent experiments. ***, $P < 0.001$ (Sidak's multiple-comparison test).

to wt. On day 10 after mosquito infection, wt oocysts grew to an average size of ~350 μm$^2$, whereas *pbgd*$^-$, *urod*$^-$, *urod*$^-_2$, and *alas*$^-$ oocysts all reached a size of only ~250 μm$^2$ (Fig. 3C). We note that size distribution was indistinguishable between mutants, consistent with their role within the same biosynthesis pathway.

When we performed the same analysis further into the oocyst maturation process 4 days later, numbers of wt, *pbgd*$^-$, and *urod*$^-$ oocysts remained similar, averaging ~100 to 200 oocysts per mosquito (see Fig. S5A and B in the supplemental material). On the other hand, analysis of oocyst sizes again revealed significant growth differences (see Fig. S5C). On day 14 after infection, wt oocysts had matured to their final size of ~600 μm$^2$. In contrast, *pbgd*$^-$ and *urod*$^-$ oocysts had grown to only ~400 μm$^2$. Most importantly, oocyst development was not completely arrested, as shown by the continuous, albeit reduced, growth of *pbgd*$^-$ and *urod*$^-$ oocysts. Together, our data show that ablation of endogenous heme biosynthesis plays no detectable role in colonization of mosquito midguts or initiation of oocyst development but leads to defective oocyst maturation.

**Impaired sporozoite production and complete life cycle arrest after disruption of *Plasmodium* heme biosynthesis in the apicoplast.** We next quantified sporozoites in *pbgd*$^-$, *urod*$^-$, *urod*$^-_2$, and *alas*$^-$ oocysts in comparison to wt-infected *Anopheles* mosquitoes (Fig. 4). In good agreement with the small oocyst size, we detected a large (~10- to 20-fold) reduction in the numbers of midgut-associated sporozoites (Fig. 4A). When liberated from oocysts, sporozoites had a normal size and stained prominently with mouse antisporozoite antiserum (Fig. 4B), suggesting that principal establishment of oocyst polarity and sporozoite morphogenesis are not affected by the absence of endogenous heme biosynthesis.

In striking contrast, quantification of hemocoel- and salivary gland-associated sporozoites revealed their complete absence in *pbgd*$^-$ and *urod*$^-$ infections and infections with all four ko parasite lines, respectively (Fig. 4A). The possibility of a delay in sporozoite production by the heme biosynthesis-deficient parasites was ruled out by the dissection of infected mosquito salivary glands at later time points (day 26). Complete life cycle arrest prior to salivary gland colonization was corroborated by transmission experiments (Fig. 5). Specifically, exposure to *Anopheles* mosquitoes infected with *pbgd*$^-$ and *urod*$^-$ parasites failed to establish a blood stage infection in mice (Fig. 5A). Thus, we conclude that early steps of heme biosynthesis in the apicoplast are necessary for the production of infectious sporozoites and the transmission to the mammalian host.

**Complete recovery of life cycle progression by complementation with ALA during sporogony.** To bypass the defect in sporogony and examine a potential effect of parasite heme defi-

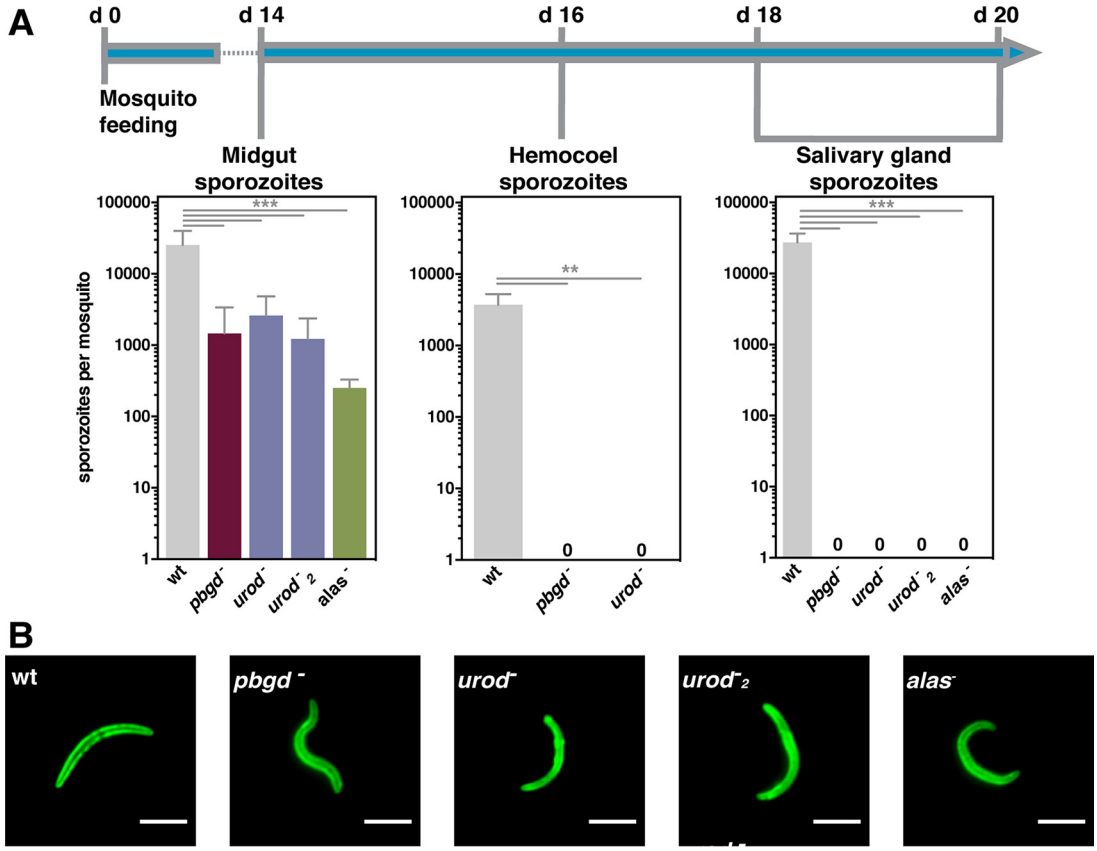


**FIG 4** Arrested sporozoite maturation in heme biosynthesis-deficient parasites. (A) Quantification of midgut-, hemocoel-, and salivary gland-associated sporozoites. Values represent mean numbers (±standard deviations) of sporozoites recovered from infected mosquito midguts, hemocoel, or salivary glands from at least three independent mosquito feeding experiments. **, $P < 0.01$; ***, $P < 0.001$ (Sidak's multiple-comparison test). (B) Normal surface staining and morphology of *pbgd*$^{-}$, *urod*$^{-}$, *urod*$^{-}_{2}$, and *alas*$^{-}$ midgut-associated sporozoites. Representative fluorescent images of wt and knockout sporozoites isolated from infected mosquito midguts 14 days after an infective blood meal. Sporozoites were labeled with mouse antisporozoite antiserum. Bars, 5 μm.

ciency in *Plasmodium* liver stages, we complemented *alas*$^{-}$ parasites with the product δ-aminolevulinic acid (ALA) as previously described (25). Similarly to *pbgd*$^{-}$ and *urod*$^{-}$ mutants, *alas*$^{-}$ parasites produced low sporozoite numbers that failed to reach the salivary glands (Fig. 4A). Accordingly, *alas*$^{-}$ parasites could not be transmitted to mice via natural bite (Fig. 5B). Complementation with ALA for the full length of vector stage development restored midgut- and salivary gland-associated sporozoite numbers to near-wt levels (see Fig. S6 in the supplemental material).

Moreover, natural mosquito transmission of complemented *alas*$^{-}$ parasites resulted in a blood stage infection in the majority (~75%) of mice (Fig. 5B). This finding contrasts with an earlier study that reported absence of blood infection after mosquito transmission of complemented *alas*$^{-}$ parasite infections to outbred Swiss mice (25). Since the most likely reason for this discrepancy is the very low susceptibility of Swiss-derived outbred mice to sporozoite infections (42), we performed wt infections with Swiss mice (see Fig. S7 in the supplemental material). In good agreement with the published data (42), sporozoite-susceptible C57BL/6 mice and sporozoite-resistant outbred Swiss mice differ largely in their proportion of blood stage positive animals and prepatent periods. Accordingly, unlike C57BL/6 mice (Fig. 5B and 6A), infections of Swiss mice with high numbers of *alas*$^{-}$ sporozoites did not lead to patency (see Fig. S7). To further exclude a wt contamination of our *alas*$^{-}$ ko line, we genotyped the blood stage parasites that developed after cycling through mosquitoes supplemented with ALA and observed no changes in the *alas*$^{-}$ genotype (Fig. 2B). Finally, to exclude potential carryover of ALA, we additionally conducted transmission experiments with mosquitoes supplemented with ALA for the first 10 days of vector development only. Importantly, this did not alter blood stage infectivity of parasites in comparison to fully complemented *alas*$^{-}$ parasites (Fig. 5B). We conclude that bypassing the defects of *alas*$^{-}$ parasites during sporogony results in infectious sporozoites, which are able to complete liver stage development without an intact pathway for parasite heme synthesis.

In stark contrast to omitting ALA supplementation late in the vector stage, omitting ALA during the first 10 days of *alas*$^{-}$ parasite development in the mosquito resulted in failure to establish a blood infection in >50% of the mice (Fig. 5B). Together, our findings show that timing of ALA complementation affected sporozoite infectivity and that endogenous synthesis of ALA is essential only for sporogony.

**Prominent auxiliary but dispensable role for parasite δ-aminolevulinic acid synthesis during liver stage development.** We next performed intravenous injections of 10,000 salivary gland sporozoites into susceptible C57BL/6 mice to corroborate our findings from natural transmission. All mice injected with com-

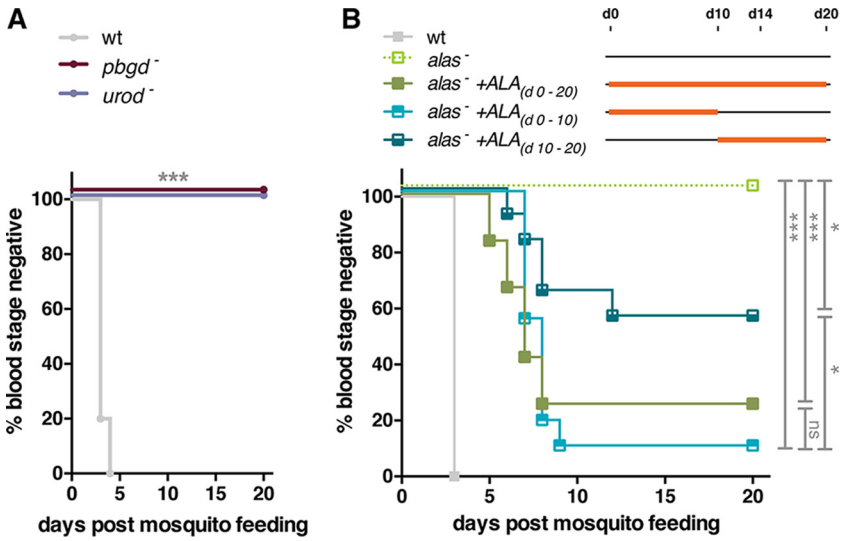


**FIG 5** Rescue of *alas*$^-$ defects by ALA supplementation during sporogony. (A) Kaplan-Meier analysis of time to blood stage infection upon natural transmission. Mice were exposed to mosquitoes infected with wt ($n = 5$) or *pbgd*$^-$ or *urod*$^-$ ($n = 11$ each) parasites. Parasitemia was followed by microscopic examination of daily Giemsa-stained thin blood films in two independent experiments. ***, $P < 0.001$ (Mantel-Cox and Gehan-Breslow-Wilcoxon tests). (B) Kaplan-Meier analysis of time to blood stage infection. Mice were exposed to mosquitoes infected with wt ($n = 9$) or *alas*$^-$ parasites that received different levels of ALA complementation ($n = 11$ per group). Parasitemias were followed by microscopic examination of daily Giemsa-stained blood films in at least two independent experiments. All survival curves of *alas*$^-$ parasites differed significantly from wt ($P < 0.001$). ns, not significant; *, $P < 0.05$; ***, $P < 0.001$ (Mantel-Cox and Gehan-Breslow-Wilcoxon tests).

plemented *alas*$^-$ sporozoites developed a blood stage infection with an average delay of 3 days, compared to wt-infected mice (Fig. 6A). Importantly, *alas*$^-$ parasites could be complemented *in vivo* by supplementing the drinking water of infected mice with ALA. This complementation led to a substantial reduction in the time to patency of *alas*$^-$ parasites, as blood stage parasites were detectable as early as 4 days after infection (Fig. 6A), demonstrating that liver stage parasites can scavenge exogenous ALA. In agreement with our past observations (43), a slow onset of blood stage infection correlated with a lack of symptoms associated with experimental cerebral malaria (ECM) (see Fig. S8 in the supplemental material). Consistent with our previous results, blood stage growth of *alas*$^-$ parasites was comparable to that of wt parasites (Fig. 6B). To examine the *in vivo* liver stage development of heme biosynthesis-deficient parasites, we next used qPCR to quantify the parasite load in livers of infected mice. As expected

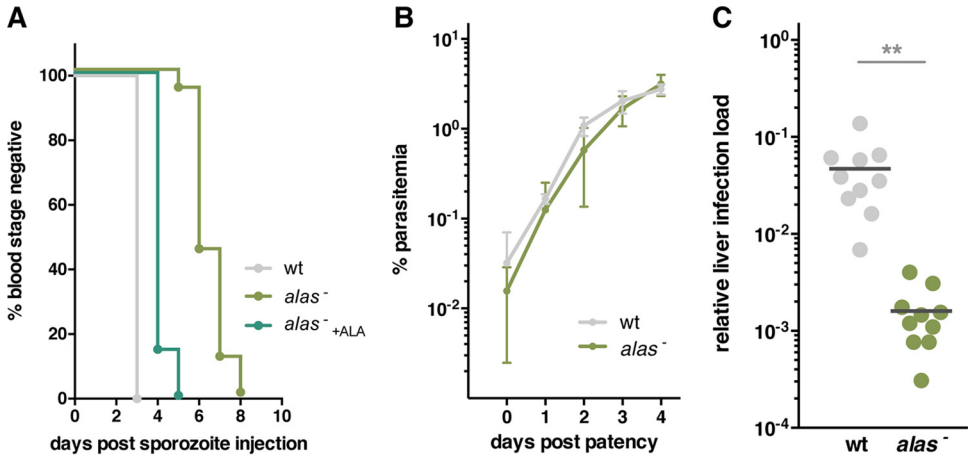


**FIG 6** *alas*$^-$ parasites can complete liver stage development *in vivo*. (A) Kaplan-Meier analysis of time to blood stage infection. Mice were intravenously injected with 10,000 wt or *alas*$^-$ sporozoites, with or without ALA supplementation. Parasitemia was followed by microscopic examination of daily Giemsa-stained blood films. Shown are data from three independent experiments; wt, $n = 9$; *alas*$^-$, $n = 18$; *alas*$^-_{+\mathrm{ALA}}$, $n = 7$. All survival curves differ from each other significantly ($P < 0.001$, Mantel-Cox and Gehan-Breslow-Wilcoxon tests). (B) Asexual blood stage development following intravenous injection of 10,000 sporozoites. Parasitemia of recipient mice was monitored daily by examination of Giemsa-stained blood smears. Shown is mean parasitemia (±standard deviation) as a function of time after patency. Data from two independent experiments; wt, $n = 5$; *alas*$^-$, $n = 16$. Differences were not significant (two-way analysis of variance). (C) Quantification of liver infection load after sporozoite infection. Parasite liver load was determined by qPCR analysis of infected mouse livers ($n = 10$ per group) harvested 42 h after intravenous injection of 10,000 wt or ALA-complemented *alas*$^-$ sporozoites. Shown are the results from two independent experiments, each conducted in triplicate. Relative expression of *P. berghei* 18S rRNA is normalized to mouse *GAPDH* transcript levels. **, $P < 0.01$ (two-way analysis of variance).

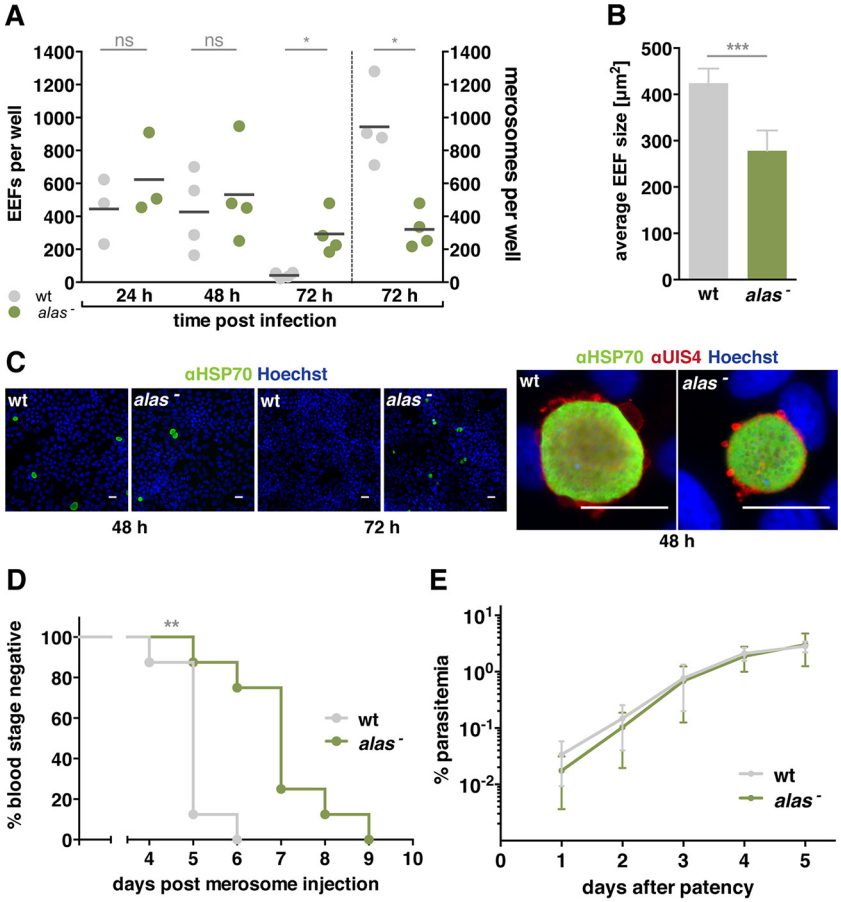


**FIG 7** Reduced liver stage maturation in *alas*⁻ parasites. (A) Quantification of exoerythrocytic forms (EEFs) and merosomes in cultured hepatoma cells at 24, 48, and 72 h after infection with 10,000 wt or *alas*⁻ sporozoites. Values represent mean numbers (±standard deviations) from at least three independent experiments. ns, not significant, *, $P < 0.05$ (two-tailed Mann-Whitney test). (B) Quantification of liver stage size in hepatoma cells 48 h after infection with 10,000 wt or *alas*⁻ sporozoites. Values represent mean size (±standard deviation) from three independent experiments and >60 EEFs each. ***, $P < 0.001$ (two-way analysis of variance). (C) Representative images of liver stages at time points indicated. Intracellular parasites were labeled with monoclonal mouse anti-*Pb*HSP70 and polyclonal rabbit anti-*Pb*UIS4 (right) primary antibodies, followed by Alexa 488- or Alexa 546-conjugated secondary antibodies and Hoechst staining. Bars, 30 μm. (D) Kaplan-Meier analysis of time to blood stage infection after intravenous injection of 180 wt or *alas*⁻ merosomes into mice ($n = 8$ per group). Parasitemia was monitored by microscopic examination of daily Giemsa-stained blood films. **, $P < 0.001$ (Gehan-Breslow-Wilcoxon test). (E) Mean parasitemia (±standard deviation) of wt and *alas*⁻ blood infections as a function of time after patency. Data are from two independent experiments. Differences were not significant (two-way analysis of variance).

from the delay in patency, the parasite load was significantly lower in the absence of ALAS (Fig. 6C).

Since our *in vivo* findings established a prominent, albeit nonlethal, deficiency in the preerythrocytic stage, we examined the infectivity and development of the knockout parasites more closely *in vitro*. First, we determined the infectivity of *alas*⁻ sporozoites in cultured hepatoma cells (Fig. 7A). At early time points (24 and 48 h postinfection), we found similar numbers of ko- and wt-infected cells, indicating that *alas*⁻ sporozoites enter hepatoma cells efficiently. Quantification of sizes of exoerythrocytic forms (EEFs) revealed that ALAS-deficient EEFs were significantly smaller than wt (Fig. 7B and C). In line with this observation, we found that 72 h after sporozoite inoculation, *alas*⁻ EEFs were still abundantly present in the infected culture, whereas wt parasites had already formed membrane-bound first-generation merozoites, termed merosomes, and had egressed from host cells (Fig. 7A and C). Despite this defect, *alas*⁻ parasites still formed merosomes, albeit in lower numbers (Fig. 7A). To determine the infectivity of *alas*⁻ merosomes, we harvested them from the culture supernatant and intravenously injected them into mice. We noticed an average delay of 2 days in mice that received *alas*⁻ merosomes compared to wt (Fig. 7D), but blood infection progressed normally (Fig. 7E).

In conclusion, our data show that during liver stage development *Plasmodium* benefits from but does not strictly rely upon endogenous synthesis of δ-aminolevulinic acid.

**Contribution of host heme biosynthesis to liver stage maturation.** To evaluate a potential role of host heme biosynthesis for maturation of liver stage parasites, we used siRNA to disrupt the host pathway at its rate-limiting step (Fig. 8). When hepatoma cells transfected with three independent, specific siRNAs against human *ALAS1* were infected with *alas*⁻ parasites, we observed an additive growth defect resulting in a significant ($P < 0.02$) decrease in parasite size with all three siRNAs compared to a negative control (Fig. 8C and E). This finding points to a contribution of an intact host heme synthesis pathway to liver stage development.

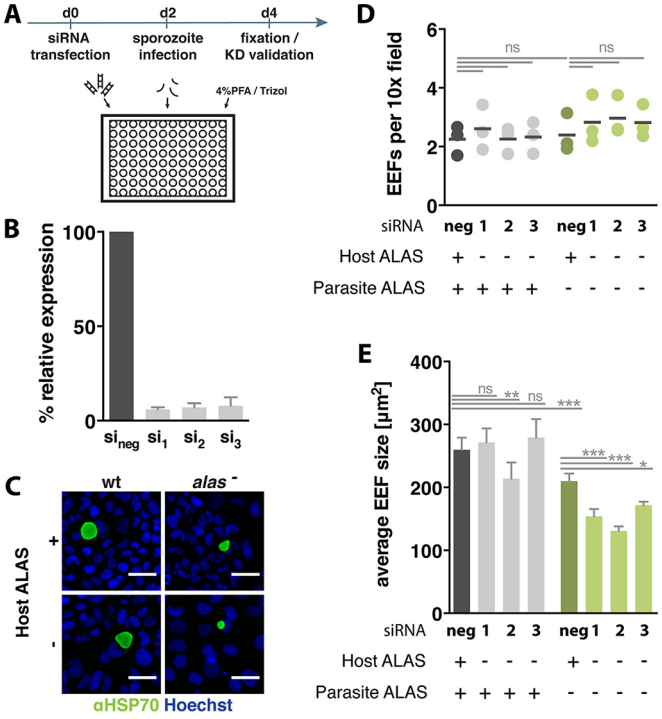


**FIG 8** Additive defects in *alas*⁻ infections of siRNA-treated hepatoma cells. (A) Experiment timeline for siRNA knockdowns (KDs). Cells were reverse transfected with different siRNAs on 96-well plates (d0) and infected with 5,000 sporozoites per well 48 h later (d2). Cells were either fixed for staining or harvested for knockdown validation 48 h postinfection (d4). (B) Transcript levels of host *ALAS1*, after transfection with three different target-specific siRNAs ($si_1$ to $si_3$), compared to a negative control ($si_{neg}$). Shown is the mean relative expression (±standard deviation) from two independent experiments, done in triplicate. Expression was normalized to human RPL13 transcript levels. Values are expressed as percentage of the negative control. (C) Representative images of EEFs, 48 h after siRNA knockdown of *ALAS1* and subsequent infection with wt or *alas*⁻ sporozoites. Samples were labeled with monoclonal mouse anti-*Pb*HSP70, followed by Alexa 488-conjugated secondary antibodies and Hoechst staining. Bars, 50 µm. (D) Quantification of exoerythrocytic forms (EEFs), after siRNA knockdown of *ALAS1* in cultured hepatoma cells, 48 h after infection with 5,000 wt (gray) or *alas*⁻ (green) sporozoites. Values represent mean parasite numbers (±standard deviation) per field of a 10× objective from three independent experiments. ns, $P > 0.1$ (two-way analysis of variance). (E) Quantification of EEF size in hepatoma cells 48 h after infection with 5,000 wt (gray) or *alas*⁻ (green) sporozoites. A minimum of 60 EEFs was quantified in each of three independent experiments. Values represent mean size (±standard deviation). ***, $P < 0.001$; **, $P < 0.01$; *, $P < 0.05$; ns, not significant (two-way analysis of variance).

Nevertheless, *alas*⁻ liver stages still reached a substantial size in ALAS-depleted hepatoma cells (Fig. 8C and E). In contrast to parasites with an impaired heme biosynthesis, growth of wt parasites was not affected by knockdown of human *ALAS1* (2 out of 3 siRNAs), suggesting that wt parasites do not strictly rely on exogenous heme or heme intermediates (Fig. 8E). Similarly, numbers of liver stage parasites remained normal regardless of the absence of either host or parasite ALAS (Fig. 8D), fully supporting our finding that a disrupted *Plasmodium* heme synthesis pathway does not impair efficient hepatocyte invasion (Fig. 7A). As suggested by the specific phenotypic changes induced by *ALAS1* knockdown, we could verify a reduction in transcript levels by >90% in siRNA-treated cells compared to the negative control (Fig. 8B).

Together, our data indicate that disruption of either endogenous or host heme biosynthesis alone does not lead to a robust life cycle arrest in the liver. Finally, our findings illustrate the metabolic flexibility of *Plasmodium* liver stages that can utilize host resources to complement or substitute endogenous synthesis of ALA.

## DISCUSSION

The most important findings from our study are a distinct vital role of endogenous *Plasmodium* heme biosynthesis in sporozoite maturation and an important auxiliary, albeit dispensable, role of the rate-limiting enzyme of the pathway, ALAS, in liver stage maturation.

Despite previous assumptions, recent advancements have revealed that *Plasmodium de novo* heme biosynthesis is an unsuitable target for conventional blood stage interventions (25, 26, 29). A recent study has proposed targeting parasite heme biosynthesis in the liver stage as an alternative therapeutic strategy (25). In contrast to the previous study, we consistently detected blood stage infections in mice inoculated with *alas*⁻ sporozoites. We have shown that this discrepancy can likely be attributed to the previous use of outbred Swiss mice, which are almost refractory to expansion of wt parasites in the liver. An additional impairment of *alas*⁻ parasites, as reported in our study, can lead to a complete liver stage arrest in a nonmatched parasite-host system. Using C57BL/6 mice, which are susceptible to sporozoite infections (42), we can refute development of *alas*⁻ sporozoites as a candidate for genetically attenuated parasites (GAPs). Moreover, we could demonstrate that infection of hepatoma cells with *alas*⁻ sporozoites leads to the formation of infectious merosomes. These merosomes also caused a blood stage infection when harvested from cultured cell supernatants and injected into mice. The observed delay in patency is consistent with our results from sporozoite injections and quantification of parasite liver load. We speculate that limited availability of heme likely impairs the function of the ETC and, by extension, affects pyrimidine synthesis or ATP-dependent processes, such as mitosis and cytokinesis.

Recent studies strongly suggest that *Plasmodium* parasites have mechanisms for the scavenging of host heme from infected erythrocytes (25, 26, 29). While heme availability is lower in the hepatocyte host, we provide evidence that an intact host pathway can contribute to liver stage development. In blood stages, parasites have the capacity to import and utilize intermediates of heme biosynthesis that were produced by host enzymes (29), a scenario which could apply to liver stage parasites as well. Our data strongly suggest that liver stage *Plasmodium* can scavenge ALA from the host environment. Whether liver stage parasites can also import heme or other heme intermediates and whether scavenging is constitutive in wt parasites or specifically regulated in the absence of endogenous resources remain interesting questions for future studies.

All three mutants that we generated in the present study displayed a distinct and complete life cycle arrest between midgut-associated sporozoites and salivary gland invasion. It is important to highlight that previous studies reported a failure in oocyst formation (25, 26), which we can confidently exclude. One explanation for this discrepancy is that different methods were used for oocyst quantification. A clear distinction between oocysts and vacuolar cells of *Anopheles* midguts remains challenging with traditional staining methods, particularly when oocyst sizes are affected. We show for the first time that infections with *pbgd*⁻, *urod*⁻, and *alas*⁻ parasites lead to normal mosquito midgut colo-

nization and an impairment in oocyst maturation. Despite this defect, mutant oocysts can produce sporozoites, but these do not seem to be released into the mosquito hemocoel and, as a consequence, cannot colonize the final organ, salivary glands. We also note that *alas*$^{-}$ parasites responded differently to early versus late complementation with ALA in the mosquito. Although this differential treatment led to the production of comparable sporozoite numbers, *alas*$^{-}$ parasites that lacked ALA during the first 10 days of their vector stage development did not infect mice as efficiently. While this finding indicates a particular reliance on the endogenous synthesis of ALA in the early stages of oocyst maturation, further investigation is needed to resolve this observation.

By targeted deletion of *PBGD* and *UROD*, our study has also substantiated a role for apicoplast-localized proteins in parasite development in the mosquito. We wish to note that our attempts to delete the third apicoplast-localized heme biosynthesis enzyme, δ-aminolevulinic acid dehydratase (ALAD), were unsuccessful. While we cannot formally exclude inaccessibility of the *ALAD* locus to gene manipulation, we consider it likely that this gene is indispensable for asexual blood stage growth. ALAD shares its apicoplast-targeting sequence with a stromal processing peptidase (SPP) through an alternative splice site (44) (see Fig. S2A in the supplemental material), and precise mutations of the two alternative splice products are needed to disentangle the individual roles for parasite propagation. The majority of apicoplast-localized proteins appear to be essential either for blood infection (e.g., key enzymes of [Fe-S] biosynthesis [45]) or during liver stage development (e.g., pyruvate dehydrogenase [PDH] [46], *Plasmodium*-specific apicoplast protein important for liver merozoite formation [PALM] [43], and enzymes of phosphatidic acid biosynthesis [47]). Together with FABI and FABB/F of the fatty acid biosynthesis pathway (48), PBGD and UROD are the first apicoplast proteins with distinct essential functions during vector stage development, highlighting the specific roles of apicoplast metabolism at various phases in the complex life cycle.

Collectively, our findings show that enzymes of *Plasmodium* heme biosynthesis are essential only for oocyst and sporozoite maturation. An intact parasite pathway for heme biosynthesis and the endogenous synthesis of ALA are beneficial but not essential during liver stage development. Together, our experimental genetics study exemplifies that metabolic flexibility varies greatly depending on the host and life cycle progression and that robust phenotyping assays are vital for target validation.

## ACKNOWLEDGMENTS

We acknowledge the assistance of the FCCF at the Deutsches Rheuma-Forschungszentrum (Berlin). We also thank Elena Levashina (MPI-IB, Germany) for the use of the epifluorescence microscope.

## FUNDING INFORMATION

This study was supported by the Max Planck Society and partly by the European Commission through the EviMalaR Network (partner 34).

## REFERENCES

1. **Ponka P.** 1999. Cell biology of heme. Am J Med Sci **318:**241–256. http://dx.doi.org/10.1016/S0002-9629(15)40628-7.
2. **Kořený L, Sobotka R, Kovářová J, Gnipová A, Flegontov P, Horváth A, Oborník M, Ayala FJ, Lukeš J.** 2012. Aerobic kinetoplastid flagellate *Phytomonas* does not require heme for viability. Proc Natl Acad Sci U S A **109:**3808–3813. http://dx.doi.org/10.1073/pnas.1201089109.
3. **Goldberg DE.** 2005. Hemoglobin degradation. Curr Top Microbiol Immunol **295:**275–291.
4. **Sadrzadeh SM, Graf E, Panter SS, Hallaway PE, Eaton JW.** 1984. Hemoglobin. A biologic Fenton reagent. J Biol Chem **259:**14354–14356.
5. **Pagola S, Stephens PW, Bohle DS, Kosar AD, Madsen SK.** 2000. The structure of malaria pigment beta-haematin. Nature **404:**307–310. http://dx.doi.org/10.1038/35005132.
6. **Sigala PA, Goldberg DE.** 2014. The peculiarities and paradoxes of *Plasmodium* heme metabolism. Annu Rev Microbiol **68:**259–278. http://dx.doi.org/10.1146/annurev-micro-091313-103537.
7. **Gardner MJ, Hall N, Fung E, White O, Berriman M, Hyman RW, Carlton JM, Pain A, Nelson KE, Bowman S, Paulsen IT, James K, Eisen JA, Rutherford K, Salzberg SL, Craig A, Kyes S, Chan M-S, Nene V, Shallom SJ, Suh B, Peterson J, Angiuoli S, Pertea M, Allen J, Selengut J, Haft D, Mather MW, Vaidya AB, Martin DMA, Fairlamb AH, Fraunholz MJ, Roos DS, Ralph SA, McFadden GI, Cummings LM, Subramanian GM, Mungall C, Venter JC, Carucci DJ, Hoffman SL, Newbold C, Davis RW, Fraser CM, Barrell B.** 2002. Genome sequence of the human malaria parasite *Plasmodium falciparum*. Nature **419:**498–511. http://dx.doi.org/10.1038/nature01097.
8. **van Dooren GG, Kennedy AT, McFadden GI.** 2012. The use and abuse of heme in apicomplexan parasites. Antioxid Redox Signal **17:**634–656. http://dx.doi.org/10.1089/ars.2012.4539.
9. **van Dooren GG, Striepen B.** 2013. The algal past and parasite present of the apicoplast. Annu Rev Microbiol **67:**271–289. http://dx.doi.org/10.1146/annurev-micro-092412-155741.
10. **Dhanasekaran S, Chandra NR, Chandrasekhar Sagar BK, Rangarajan PN, Padmanaban G.** 2004. Delta-aminolevulinic acid dehydratase from *Plasmodium falciparum*: indigenous versus imported. J Biol Chem **279:**6934–6942. http://dx.doi.org/10.1074/jbc.M311409200.
11. **Sato S, Clough B, Coates L, Wilson RJM.** 2004. Enzymes for heme biosynthesis are found in both the mitochondrion and plastid of the malaria parasite *Plasmodium falciparum*. Protist **155:**117–125. http://dx.doi.org/10.1078/1434461000169.
12. **Nagaraj VA, Arumugam R, Chandra NR, Prasad D, Rangarajan PN, Padmanaban G.** 2009. Localisation of *Plasmodium falciparum* uroporphyrinogen III decarboxylase of the heme-biosynthetic pathway in the apicoplast and characterisation of its catalytic properties. Int J Parasitol **39:**559–568. http://dx.doi.org/10.1016/j.ijpara.2008.10.011.
13. **Varadharajan S, Dhanasekaran S, Bonday ZQ, Rangarajan PN, Padmanaban G.** 2002. Involvement of delta-aminolaevulinate synthase encoded by the parasite gene in de novo haem synthesis by *Plasmodium falciparum*. Biochem J **367:**321–327. http://dx.doi.org/10.1042/bj20020834.
14. **Nagaraj VA, Prasad D, Rangarajan PN, Padmanaban G.** 2009. Mitochondrial localization of functional ferrochelatase from *Plasmodium falciparum*. Mol Biochem Parasitol **168:**109–112. http://dx.doi.org/10.1016/j.molbiopara.2009.05.008.
15. **Nagaraj VA, Prasad D, Arumugam R, Rangarajan PN, Padmanaban G.** 2010. Characterization of coproporphyrinogen III oxidase in *Plasmodium falciparum* cytosol. Parasitol Int **59:**121–127. http://dx.doi.org/10.1016/j.parint.2009.12.001.
16. **Kořený L, Oborník M, Lukeš J.** 2013. Make it, take it, or leave it: heme metabolism of parasites. PLoS Pathog **9:**e1003088. http://dx.doi.org/10.1371/journal.ppat.1003088.
17. **Painter HJ, Morrisey JM, Mather MW, Vaidya AB.** 2007. Specific role of mitochondrial electron transport in blood-stage *Plasmodium falciparum*. Nature **446:**88–91. http://dx.doi.org/10.1038/nature05572.
18. **Vaidya AB, Painter HJ, Morrisey JM, Mather MW.** 2008. The validity of mitochondrial dehydrogenases as antimalarial drug targets. Trends Parasitol **24:**8–9. http://dx.doi.org/10.1016/j.pt.2007.10.005.
19. **Fry M, Pudney M.** 1992. Site of action of the antimalarial hydroxynaphthoquinone, 2-[trans-4-(4′-chlorophenyl) cyclohexyl]-3-hydroxy-1,4-naphthoquinone (566C80). Biochem Pharmacol **43:**1545–1553. http://dx.doi.org/10.1016/0006-2952(92)90213-3.
20. **Srivastava IK, Rottenberg H, Vaidya AB.** 1997. Atovaquone, a broad spectrum antiparasitic drug, collapses mitochondrial membrane potential in a malarial parasite. J Biol Chem **272:**3961–3966. http://dx.doi.org/10.1074/jbc.272.7.3961.
21. **Kessl JJ, Lange BB, Mercer J, Zwicker K, Hill P, Meunier B, Pálsdóttir H, Hunte C, Meshnick S, Trumpower BL.** 2003. Molecular basis for atovaquone binding to the cytochrome bc1 complex. J Biol Chem **278:**31312–31318. http://dx.doi.org/10.1074/jbc.M304042200.
22. **Cassera MB, Zhang Y, Hazleton KZ, Schramm VL.** 2011. Purine and pyrimidine pathways as targets in *Plasmodium falciparum*. Curr Top Med Chem **11:**2103–2115. http://dx.doi.org/10.2174/156802611796575948.

23. **Boysen KE, Matuschewski K.** 2011. Arrested oocyst maturation in *Plasmodium* parasites lacking type II NADH:ubiquinone dehydrogenase. J Biol Chem **286:**32661–32671. http://dx.doi.org/10.1074/jbc.M111.269399.
24. **Sturm A, Mollard V, Cozijnsen A, Goodman CD, McFadden GI.** 2015. Mitochondrial ATP synthase is dispensable in blood-stage *Plasmodium berghei* rodent malaria but essential in the mosquito phase. Proc Natl Acad Sci U S A **112:**10216–10223. http://dx.doi.org/10.1073/pnas.1423959112.
25. **Nagaraj VA, Sundaram B, Varadarajan NM, Subramani PA, Kalappa DM, Ghosh SK, Padmanaban G.** 2013. Malaria parasite-synthesized heme is essential in the mosquito and liver stages and complements host heme in the blood stages of infection. PLoS Pathog **9:**e1003522. http://dx.doi.org/10.1371/journal.ppat.1003522.
26. **Ke H, Sigala PA, Miura K, Morrisey JM, Mather MW, Crowley JR, Henderson JP, Goldberg DE, Long CA, Vaidya AB.** 2014. The heme biosynthesis pathway is essential for *Plasmodium falciparum* development in mosquito stage but not in blood stages. J Biol Chem **289:**34827–34837. http://dx.doi.org/10.1074/jbc.M114.615831.
27. **Surolia N, Padmanaban G.** 1992. De novo biosynthesis of heme offers a new chemotherapeutic target in the human malarial parasite. Biochem Biophys Res Commun **187:**744–750. http://dx.doi.org/10.1016/0006-291X(92)91258-R.
28. **Smith CM, Jerkovic A, Puy H, Winship I, Deybach J-C, Gouya L, van Dooren G, Goodman CD, Sturm A, Manceau H, McFadden GI, David P, Mercereau-Puijalon O, Burgio G, McMorran BJ, Foote SJ.** 2015. Red cells from ferrochelatase-deficient erythropoietic protoporphyria patients are resistant to growth of malarial parasites. Blood **125:**534–541. http://dx.doi.org/10.1182/blood-2014-04-567149.
29. **Sigala PA, Crowley JR, Henderson JP, Goldberg DE.** 2015. Deconvoluting heme biosynthesis to target blood-stage malaria parasites. eLife **4:**e09143. http://dx.doi.org/10.7554/eLife.09143.
30. **Matz JM, Matuschewski K, Kooij TWA.** 2013. Two putative protein export regulators promote *Plasmodium* blood stage development in vivo. Mol Biochem Parasitol **191:**44–52. http://dx.doi.org/10.1016/j.molbiopara.2013.09.003.
31. **Janse CJ, Franke-Fayard B, Mair GR, Ramesar J, Thiel C, Engelmann S, Matuschewski K, van Gemert GJ, Sauerwein RW, Waters AP.** 2006. High efficiency transfection of *Plasmodium berghei* facilitates novel selection procedures. Mol Biochem Parasitol **145:**60–70. http://dx.doi.org/10.1016/j.molbiopara.2005.09.007.
32. **Kooij TWA, Rauch MM, Matuschewski K.** 2012. Expansion of experimental genetics approaches for *Plasmodium berghei* with versatile transfection vectors. Mol Biochem Parasitol **185:**19–26. http://dx.doi.org/10.1016/j.molbiopara.2012.06.001.
33. **Kenthirapalan S, Waters AP, Matuschewski K, Kooij TWA.** 2012. Flow cytometry-assisted rapid isolation of recombinant *Plasmodium berghei* parasites exemplified by functional analysis of aquaglyceroporin. Int J Parasitol **42:**1185–1192. http://dx.doi.org/10.1016/j.ijpara.2012.10.006.
34. **Vanderberg JP.** 1975. Development of infectivity by the *Plasmodium berghei* sporozoite. J Parasitol **61:**43–50. http://dx.doi.org/10.2307/3279102.
35. **Lackner P, Beer R, Heussler V, Goebel G, Rudzki D, Helbok R, Tannich E, Schmutzhard E.** 2006. Behavioural and histopathological alterations in mice with cerebral malaria. Neuropathol Appl Neurobiol **32:**177–188. http://dx.doi.org/10.1111/j.1365-2990.2006.00706.x.
36. **Bruña-Romero O, Hafalla JC, Gonzalez-Aseguinolaza G, Sano G-I, Tsuji M, Zavala F.** 2001. Detection of malaria liver-stages in mice infected through the bite of a single Anopheles mosquito using a highly sensitive real-time PCR. Int J Parasitol **31:**1499–1502. http://dx.doi.org/10.1016/S0020-7519(01)00265-X.
37. **Friesen J, Silvie O, Putrianti ED, Hafalla JCR, Matuschewski K, Borrmann S.** 2010. Natural immunization against malaria: causal prophylaxis with antibiotics. Sci Transl Med **2:**40ra49. http://dx.doi.org/10.1126/scitranslmed.3001058.
38. **Hliscs M, Nahar C, Frischknecht F, Matuschewski K.** 2013. Expression profiling of *Plasmodium berghei* HSP70 genes for generation of bright red fluorescent parasites. PLoS One **8:**e72771. http://dx.doi.org/10.1371/journal.pone.0072771.
39. **Silvie O, Goetz K, Matuschewski K.** 2008. A sporozoite asparagine-rich protein controls initiation of *Plasmodium* liver stage development. PLoS Pathog **4:**e1000086. http://dx.doi.org/10.1371/journal.ppat.1000086.
40. **Potocnjak P, Yoshida N, Nussenzweig RS, Nussenzweig V.** 1980. Monovalent fragments (Fab) of monoclonal antibodies to a sporozoite surface antigen (Pb44) protect mice against malarial infection. J Exp Med **151:**1504–1513. http://dx.doi.org/10.1084/jem.151.6.1504.
41. **Müller K, Matuschewski K, Silvie O.** 2011. The Puf-family RNA-binding protein Puf2 controls sporozoite conversion to liver stages in the malaria parasite. PLoS One **6:**e19860. http://dx.doi.org/10.1371/journal.pone.0019860.
42. **Scheller LF, Wirtz RA, Azad AF.** 1994. Susceptibility of different strains of mice to hepatic infection with *Plasmodium* berghei. Infect Immun **62:**4844–4847.
43. **Haussig JM, Matuschewski K, Kooij TWA.** 2011. Inactivation of a *Plasmodium* apicoplast protein attenuates formation of liver merozoites. Mol Microbiol **81:**1511–1525. http://dx.doi.org/10.1111/j.1365-2958.2011.07787.x.
44. **van Dooren GG, Su V, D'Ombrain MC, McFadden GI.** 2002. Processing of an apicoplast leader sequence in *Plasmodium falciparum* and the identification of a putative leader cleavage enzyme. J Biol Chem **277:**23612–23619. http://dx.doi.org/10.1074/jbc.M201748200.
45. **Haussig JM, Matuschewski K, Kooij TWA.** 2014. Identification of vital and dispensable sulfur utilization factors in the *Plasmodium* apicoplast. PLoS One **9:**e89718. http://dx.doi.org/10.1371/journal.pone.0089718.
46. **Pei Y, Tarun AS, Vaughan AM, Herman RW, Soliman JMB, Erickson-Wayman A, Kappe SHI.** 2010. *Plasmodium* pyruvate dehydrogenase activity is only essential for the parasite's progression from liver infection to blood infection. Mol Microbiol **75:**957–971. http://dx.doi.org/10.1111/j.1365-2958.2009.07034.x.
47. **Lindner SE, Sartain MJ, Hayes K, Harupa A, Moritz RL, Kappe SHI, Vaughan AM.** 2014. Enzymes involved in plastid-targeted phosphatidic acid synthesis are essential for *Plasmodium yoelii* liver-stage development. Mol Microbiol **91:**679–693. http://dx.doi.org/10.1111/mmi.12485.
48. **van Schaijk BCL, Kumar T, Vos MW, Richman A, van Gemert GJ, Li T, Eappen AG, Williamson KC, Morahan BJ, Fishbaugher M, Kennedy M, Camargo N, Khan SM, Janse CJ, Sim KL, Hoffman SL, Kappe SHI, Sauerwein RW, Fidock DA, Vaughan AM.** 2014. Type II fatty acid biosynthesis is essential for *Plasmodium falciparum* sporozoite development in the midgut of Anopheles mosquitoes. Eukaryot Cell **13:**550–559. http://dx.doi.org/10.1128/EC.00264-13.